Enhanced Photocatalytic Hydrogen Evolution over Cu−Doped ZnIn2S4 under Visible Light Irradiation

ARTICLE *in* THE JOURNAL OF PHYSICAL CHEMISTRY C · SEPTEMBER 2008

Impact Factor: 4.77 · DOI: 10.1021/jp804525q

4 AUTHORS, INCLUDING:

Liang Zhao
Xi'an Jiaotong University
48 PUBLICATIONS **835** CITATIONS
SEE PROFILE

Zhaohui Zhou
Xi'an Jiaotong University
22 PUBLICATIONS **294** CITATIONS
SEE PROFILE

Liejin Guo
Xi'an Jiaotong University
337 PUBLICATIONS **8,033** CITATIONS
SEE PROFILE

Enhanced Photocatalytic Hydrogen Evolution over Cu-Doped $ZnIn_2S_4$ under Visible Light Irradiation

Shaohua Shen, Liang Zhao,* Zhaohui Zhou, and Liejin Guo

State Key Laboratory of Multiphase Flow in Power Engineering, Xi'an Jiaotong University, Xi'an, ShaanXi 710049, P. R. China

Received: May 22, 2008; Revised Manuscript Received: July 25, 2008

A series of Cu-doped $ZnIn_2S_4$ photocatalysts has been synthesized by a facile hydrothermal method, with the copper concentration varying from 0 wt% to 2.0 wt%. The physical and photophysical properties of these Cu-doped $ZnIn_2S_4$ photocatalysts were characterized by X-ray diffraction (XRD), photoluminescence spectroscopy (PL), scanning electron microscopy (SEM), and UV−visible diffuse reflectance spectroscopy (UV−vis). The diffuse reflectance and photoluminescence spectra of Cu-doped $ZnIn_2S_4$ shifted monotonically to longer wavelengths as the copper concentration increased from 0 wt% to 2.0 wt%, indicating that the optical properties of these photocatalysts greatly depended on the amount of Cu doped. Meanwhile, the layered structure of $ZnIn_2S_4$ would be destructed gradually by Cu doping. The photoactivity of $ZnIn_2S_4$ was enhanced when Cu^{2+} was doped into the crystal structure. The highest photocatalytic activity was observed on Cu (0.5 wt%)–doped $ZnIn_2S_4$, with the rate of hydrogen evolution to be 151.5 μmol/h under visible light irradiation ($\lambda > 430$ nm). On the basis of the calculated energy band positions and optical properties, the effect of copper as a dopant on the photocatalytic activity of Cu-$ZnIn_2S_4$ was studied.

1. Introduction

Photocatalytic water splitting into H_2 and O_2 using semiconductor photocatalysts has been regarded as an attractive solution to resolve the global energy and environmental problems. Many effective photocatalysts have been developed; however, most of them only work in the ultraviolet region because of their wide band gap.[1−4] Thus, developing highly active photocatalysts with visible light response to use solar energy is important, as the ultraviolet light occupies only 2−3% of solar energy.

Over the past few years, considerable effort has been made to narrow the band gap of catalysts to improve visible light response. Recent progress includes single-phase oxide $PbBi_2Nb_2O_9$ for isopropyl alcohol degradation and water decomposition,[5] GaN-ZnO solid solution,[6] and titanium disilicide[7] for pure water decomposition to H_2 and O_2. One effective way to increase the absorption of photocatalyst is to form donor levels in the forbidden band by introducing foreign elements into active photocatalysts with a wide band gap. TiO_2 codoped with Ni and Ta,[8] ZnS doped with Cu or Ni,[9,10] and ZnS codoped with Pb and halogens[11] have been reported as active photocatalysts under visible-light irradiation. In particular, the $InTaO_4$ doped with Ni was found to be an active photocatalyst for overall water splitting in the visible light region.[12]

On the other hand, chalcogenides such as CdS have been studied extensively, since they have ideal edge positions of the valence and conduction bands for hydrogen production from aqueous electrolyte solutions containing a sacrificial agent (Na_2S or/and Na_2SO_3) under visible light irradiation.[13,14] Unfortunately, they also have a fatal disadvantage of photocorrosion, i.e., photogenerated holes in the valence band tend to react with chalcogenides themselves.[15] Although incorporation of chalcogenides into interlayers[16] or mesoporous materials[17,18] was efficient for stabilizing the chalcogenides and producing hydrogen from water, the photocatalytic efficiency is still low. Recently, some multicomponent metal sulfides have been reported to be more stable and show higher photocatalytic activity under visible light.[19−21] Moreover, the CdZnS doped with Cu showed greatly improved stability and photocatalytic activity even without Pt as a cocatalyst.[22]

Ternary sulfide $ZnIn_2S_4$, as the only member of the AB_2X_4 family semiconductor with a layered structure, has attracted far-ranging interests because of its potential applications in different fields such as charge storage,[23] thermoelectricity,[24] and photoconduction.[25] In 2003, Lei et al.[26] synthesized $ZnIn_2S_4$ by a simple hydrothermal method and first treated $ZnIn_2S_4$ as an efficient visible-light-driven photocatalyst for hydrogen production. In 2006, Gou et al.[27] hydrothermally prepared the $ZnIn_2S_4$ solid or hollow microspheres in the presence of a surfactant such as cetyltrimethylammonium bromide (CTAB) or poly(ethylene glycol) (PEG). In our previous research,[28,29] the photocatalytic activity of $ZnIn_2S_4$ could be further enhanced when hydrothermally prepared in the presence of CTAB. Thus, $ZnIn_2S_4$ turned to be a good candidate for hydrogen production from water under visible light. In the present study, a series of $ZnIn_2S_4$ doped with different amounts of Cu was synthesized by a CTAB-assisted hydrothermal method. The effects of Cu doping on the morphology, optical properties, and photocatalytic activities of $ZnIn_2S_4$ were discussed in detail.

2. Experimental Section

2.1. Synthesis of Cu-Doped $ZnIn_2S_4$. All chemicals are of analytical grade and used as received without further purification. $ZnIn_2S_4$ products were prepared by a hydrothermal synthetic method.[27] In a typical procedure, 0.735 g of $ZnSO_4 \cdot 7H_2O$, 1.615 g of $In(NO_3)_3 \cdot 4H_2O$, 0.65 g of cetyltrimethylammonium bromide (CTAB), and a double excess of thioacetamide (TAA) were dissolved in 50 mL of distilled water. The mixed solution was then transferred into a 70-mL Teflon-lined autoclave. The autoclave was sealed and kept at 160 °C for 12 h

* To whom correspondence should be addressed. Phone: +86-29-82668287. Fax: +86-29-82669033. E-mail address: lzhao@mail.xjtu.edu.cn.

10.1021/jp804525q CCC: $40.75
Published on Web 09/20/2008

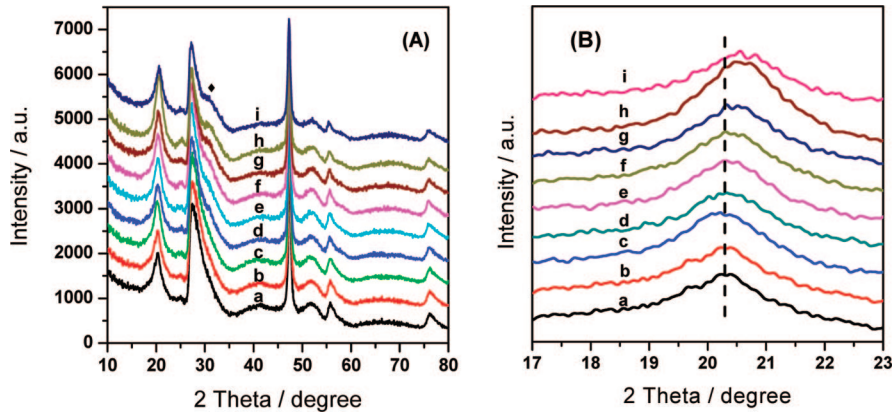

Figure 1. X-ray diffraction patterns of Cu(X)-$ZnIn_2S_4$; the values of X were (a) 0.0 wt%, (b) 0.1 wt%, (c) 0.3 wt%, (d) 0.5 wt%, (e) 0.7 wt%; (f) 0.9 wt%, (g) 1.2 wt%, (h) 1.6 wt%, (i) 2.0 wt%.

and then cooled to room temperature naturally. A yellow precipitate was obtained, which was then filtered and washed with absolute ethanol and distilled water for several times. After being dried in a vacuum at 80 °C, $ZnIn_2S_4$ was obtained. For the synthesis of Cu-doped $ZnIn_2S_4$, a desired amount of 0.1 M $Cu(NO_3)_2$ solution was added into the mixed solution before transferring into the autoclave. $ZnIn_2S_4$ doped with different amounts of Cu is denoted as Cu(X)-$ZnIn_2S_4$; the value of X, from 0 wt% to 2.0 wt%, is used to describe the weight content of Cu.

2.2. Characterization. The X-ray diffraction (XRD) patterns were obtained from a PANalytical X'pert MPD Pro diffractometer using Ni-filtered Cu Kα irradiation (Wavelength 1.5406 Å). The diffuse reflection of the samples was determined by a Hitachi U-4100 UV−vis−near-IR spectrophotometer. The analysis of photoluminescence spectra (PL) was carried out at room temperature using a PTI QM-4 fluorescence spectrophotometer. The sample morphology was observed by a JEOL JSM-6700FE scanning electron microscope.

2.3. Evaluation of Photocatalytic Activity. Photocatalytic hydrogen evolution was performed in a gas-closed circulation system with a top window Pyrex cell. A 300 W Xe lamp was used as the light source, and the UV part of the light was removed by a cutoff filter ($\lambda > 430$ nm). Hydrogen evolved was analyzed by an online thermal conductivity detector (TCD) gas chromatograph (NaX zeolite column, nitrogen as a carrier gas) every 10 min. In all experiments, the photocatalyst powder (0.2 g) was dispersed by a magnetic stirrer in 150 mL of 0.25 M Na_2SO_3/0.35 M Na_2S aqueous solution. Here, Na_2SO_3/Na_2S mixed sacrificial agent was used to scavenge photogenerated holes. Nitrogen was purged through the cell before reaction to remove oxygen. Pt (1 wt%) as a cocatalyst for the promotion of hydrogen evolution was photodeposited in situ on the photocatalysts from the precursor of $H_2PtCl_6 \cdot 6H_2O$. The temperature for all the photocatalytic reactions was kept at 25 ± 0.5 °C. The blank experiments showed no appreciable H_2 evolution in the absence of irradiation or photocatalyst. Apparent quantum yield defined by the eq 1 was measured using a 420 nm band-pass filter and an irradiatometer.

$$\text{A.Q.Y.}(\%) = \frac{\text{the number of reacted electrons}}{\text{the number of incident photons}} \times 100 = \frac{\text{the number of evolved } H_2 \text{ molecules} \times 2}{\text{the number of incident photons}} \times 100 \quad (1)$$

2.4. Band Structure Calculation. The plane-wave-based density functional theory (DFT) calculation was carried out for $ZnIn_2S_4$ with hexagonal structure by employing the CASTEP program to obtain further information about the energy structure of the Cu-$ZnIn_2S_4$ photocatalysts.[30] The core electrons were treated using ultrasoft pseudopotentials,[31] and the valence electronic configurations for Zn, In, and S are $3d^{10}4s^2$, $4d^{10}5s^25p^1$, and $3s^23p^4$, respectively. The kinetic energy cutoff was taken to be 400 eV for $ZnIn_2S_4$. The exchange and correlation interactions were modeled using the generalized gradient approximation (GGA). The calculation was carried out using the primitive unit cell of $[ZnIn_2S_4]_2$, which had 31 occupied orbitals. The atomic coordinates of $ZnIn_2S_4$ were obtained from Gou et al.[27]

3. Results and Discussion

3.1. Crystal Structure. Figure 1A shows X-ray diffraction patterns of Cu(X)-$ZnIn_2S_4$ photocatalysts (X = 0 wt% to 2.0 wt%). Without Cu doping, the diffraction peaks of the obtained $ZnIn_2S_4$ sample can be readily indexed as a pure phase hexagonal $ZnIn_2S_4$ (ICSD-JCPDS card No. 01-072-0773, a = 3.85 Å, c = 24.68 Å), and no other impurities such as ZnS, In_2S_3, oxides, or organic compounds related to reactants were detected. When $ZnIn_2S_4$ was doped with Cu, the XRD patterns of the obtained Cu(X)-$ZnIn_2S_4$ were almost the same as that of the hexagonal $ZnIn_2S_4$, except that the diffraction peaks were slightly shifted to higher angles with the amount of Cu doped increasing, as shown in Figure 1B. This observation suggested that Cu^{2+} was homogeneously incorporated into the lattice of $ZnIn_2S_4$, because the ionic radius of Cu^{2+} (0.72 Å) is smaller than the radius of Zn^{2+} (0.74 Å) and In^{3+} (0.81 Å).[32] Furthermore, Cu^{2+} may occupy the Zn^{2+} site, since charge compensation was very easy in this case, as deduced by Shionoya et al.[33] An XRD pattern of CuS around 2θ = 30° could be easily observed while the amount of Cu doped was close to 2.0 wt%. This was due to the limitation of doping amount in the $ZnIn_2S_4$ lattice.[11]

3.2. Morphology. Figure 2 shows SEM images for Cu(X)-$ZnIn_2S_4$ with X = 0 wt% to 2.0 wt%. During the hydrothermal process, addition of Cu ion directly affects the morphology of Cu-$ZnIn_2S_4$. When none of the Cu was doped, $ZnIn_2S_4$ exhibited a lot of separate microspheres with diameters of 1−2 μm, as shown in Figure 2a. Further observation showed that all the microspheres were composed of numerous petals/sheets. This growth tendency of lamellar structures might be related to the layered feature of hexagonal $ZnIn_2S_4$.[27] When X = 0.1 wt% to 0.5 wt %, $ZnIn_2S_4$ products still appeared in the shape of microspheres; however, increasing the amount of Cu doped led to gradual decrease in the diameter of Cu(X)-$ZnIn_2S_4$ microspheres. The diameter of microsphere was about 0.5−1 μm for

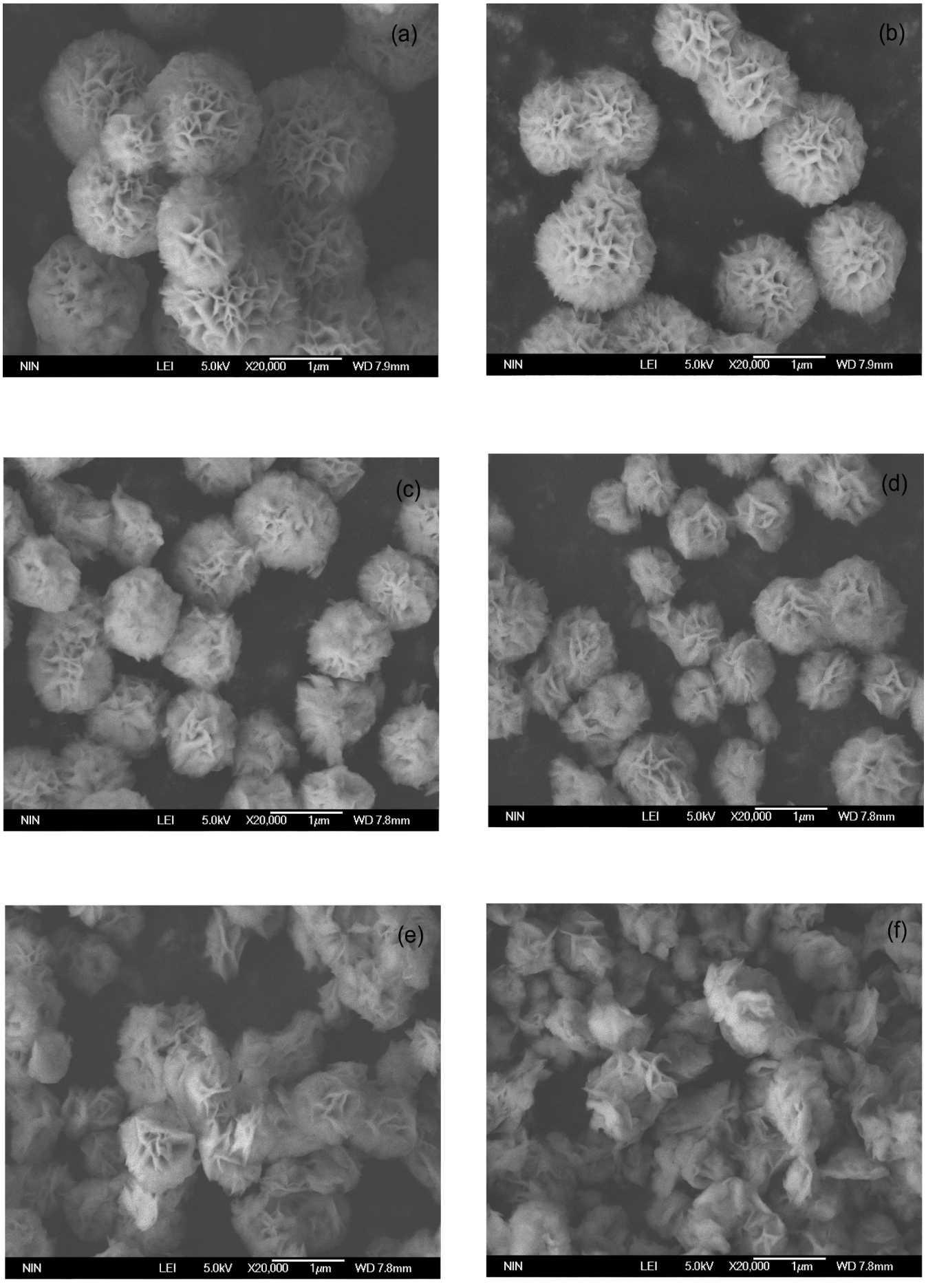

Figure 2. Part 1 of 2.

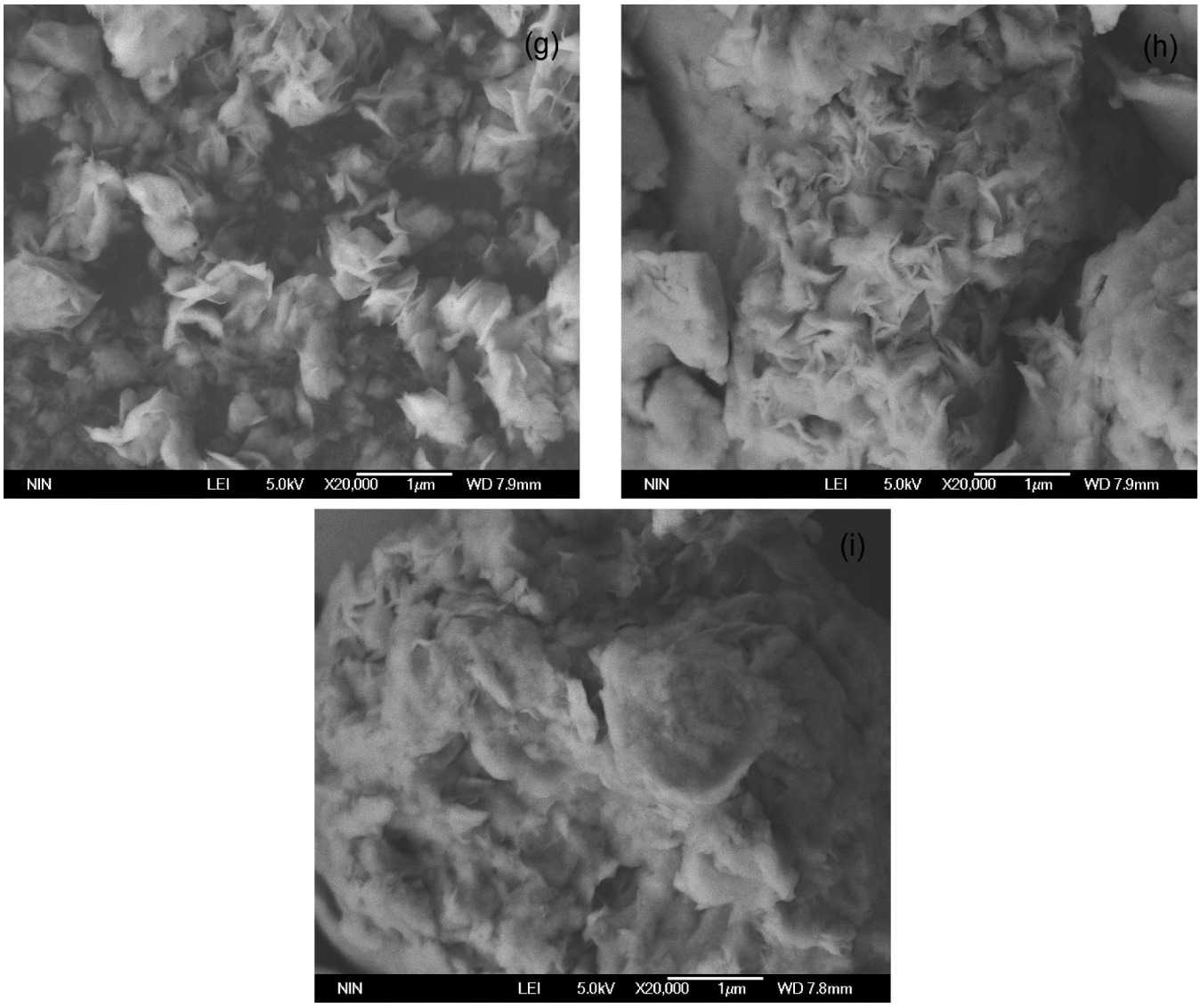

Figure 2. Part 2 of 2. Scanning electron microscope images of Cu(X)-$ZnIn_2S_4$; the values of X were (a) 0.0 wt%, (b) 0.1 wt%, (c) 0.3 wt%, (d) 0.5 wt%, (e) 0.7 wt%; (f) 0.9 wt%, (g) 1.2 wt%, (h) 1.6 wt%, (i) 2.0 wt%.

Cu(0.5 wt%)-$ZnIn_2S_4$. As X increased further, the shape of microspheres for Cu(X)-$ZnIn_2S_4$ was destructed partially and even throughly, as shown in Figure 2e−g, as well as the petals/sheets presented to be more irregular. When X = 1.6 wt% to 2.0 wt %, instead of microspheres and petals/sheets, Cu(X)-$ZnIn_2S_4$ turned out to be a bulky conglomeration with a rough surface, and petals/sheets could be hardly observed. The morphology of the Cu(X)-$ZnIn_2S_4$ samples obtained in the same synthetic condition varies regularly with the increasing amount of Cu doped. That is to say, the layered structure of hexagonal $ZnIn_2S_4$, as well as the shape of microspheres, could be destructed gradually by the increasing Cu dopant.

3.3. Optical Properties. Figure 3 shows the UV−vis diffuse reflectance spectra of Cu(X)-$ZnIn_2S_4$ with X = 0 wt% to 2.0 wt%. The onset of the absorption edge of $ZnIn_2S_4$ was at about 495 nm, corresponding to the band gap of 2.51 eV. Moreover, $ZnIn_2S_4$ had an intense absorption band with a steep edge in the visible-light region. This shape indicated that the UV−vis absorption was due to the band gap transition but not due to the transition from impurity levels to the conduction band of $ZnIn_2S_4$. As X increased, a new absorption shoulder around 500 nm was observed, and the absorption edge of Cu(X)-$ZnIn_2S_4$ shifted monotonously from 575 to 650 nm with an increase in

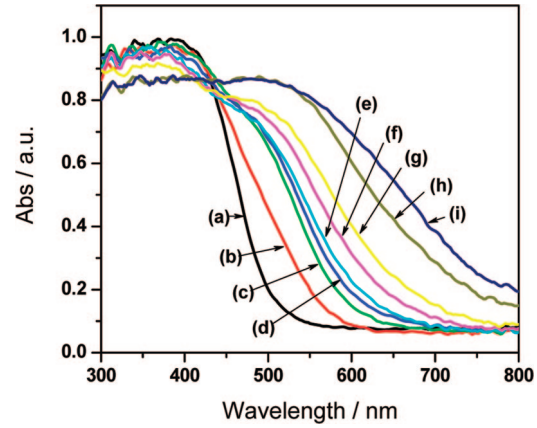

Figure 3. Diffuse reflectance spectra of Cu(X)-$ZnIn_2S_4$; the values of X were (a) 0.0 wt%, (b) 0.1 wt%, (c) 0.3 wt%, (d) 0.5 wt%, (e) 0.7 wt%; (f) 0.9 wt%, (g) 1.2 wt%, (h) 1.6 wt%, (i) 2.0 wt%.

X from 0.1 wt% to 1.2 wt%, corresponding to the narrowing of the band gap from 2.16 to 1.91 eV. The absorption shoulder with a long tail on the low energy side, which was characteristic of doped photocatalysts[34,35] and indicated that intraband gap states were formed by the dopants in the forbidden band, could

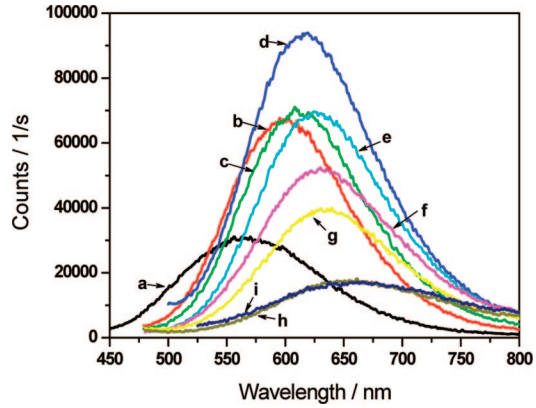

Figure 4. Photoluminescence spectra of Cu(X)-$ZnIn_2S_4$; the values of X were (a) 0.0 wt%, (b) 0.1 wt%, (c) 0.3 wt%, (d) 0.5 wt%, (e) 0.7 wt%; (f) 0.9 wt%, (g) 1.2 wt%, (h) 1.6 wt%, (i) 2.0 wt%, excited at 330 nm.

TABLE 1: Band Gap, Absorption Edge, PL Emission and Emission Intensity of Cu(X)-$ZnIn_2S_4$, with X = 0.0 wt% to 2.0 wt%

X (wt%)	band gap[a] (eV)	absorption edge (nm)	PL emission (nm)	emission intensity (normalized, a.u.)
0.0	2.51	495	560	0.33
0.1	2.16	575	597	0.72
0.3	2.11	587	611	0.76
0.5	2.05	604	617	1.00
0.7	2.02	614	626	0.74
0.9	1.94	639	632	0.56
1.2	1.91	650	639	0.42
1.6	1.73	715	655	0.20
2.0	1.65	750	666	0.19

[a] Calculated from absorption edge.

be assigned to the transition from the Cu3d level above the valence band to the conduction band of $ZnIn_2S_4$. In addition, a broad band (λ > 750 nm) was observed for Cu (1.6 wt% to 2.0 wt%)-$ZnIn_2S_4$. This was due to the impurity CuS phase, as indicated by X-ray diffraction.

The PL spectra of Cu(X)-$ZnIn_2S_4$, with X = 0 wt% to 2.0 wt%, were obtained using an excitation wavelength of 330 nm, as shown in Figure 4. The PL intensity and response range of Cu(X)-$ZnIn_2S_4$ were influenced by Cu doping. The PL spectra, in company with the diffuse reflect spectra, shifted successively to longer wavelength with the change in the amount of Cu doped, indicating that the energy structure of Cu(X)-$ZnIn_2S_4$ depended on the value of X. Similar phenomena has been reported by Kudo et al. in the $(AgIn)_xZn_{2(1-x)}S_2$ solid solutions.[19] However, as shown in Table 1, the emission spectra of Cu(X)-$ZnIn_2S_4$ (X = 0.0 wt% to 0.7 wt%) was somewhat red-shifted vis-a-vis the absorption edge. This is because the PL emission of Cu(X)-$ZnIn_2S_4$ presented here is broadband,[36] or donor−acceptor defect (such as sulfur vacancy) based,[37] in nature. In constrast, the absorption edge of Cu(X)-$ZnIn_2S_4$ (X = 0.9 wt% to 2.0 wt%) shifted to longer wavelength when compared to the emission spectra. This may be due to the excess of Cu doping, resulting in the formation of CuS, which has a total absorption in the visible-light region. Thus, as reported by Peng et al. on Cu-ZnS,[38] the PL emission of Cu(X)-$ZnIn_2S_4$ may arise from the recombination between the shallow donor level (sulfur vacancy) and the t_2 level of Cu^{2+} (splitting from Cu3d). As the energy level of sulfur vacancy relative to the valence band nearly stays constant in these samples despite the variation in Cu^{2+} concentration, it can be concluded that the t_2 energy level of Cu^{2+} ions is farther from the valence band with increasing Cu^{2+} concentration. In addition, it could be found from Figure 4 that the PL intensity of Cu(X)-$ZnIn_2S_4$ gradually increased as the Cu content increased and arrived at the highest degree when the Cu content was 0.5 wt%. While the Cu content continued to increase, namely more than 0.5 wt%, the PL intensity began to decrease. In Mn-ZnS[39] and Cu-ZnS,[38] a similar photoluminescence phenomenon was also observed, which can be explained by the effect of ion doping. As the foregoing analysis shows, these PL spectra were related to native defects (e.g., sulfur vacancy). When Cu^{2+} was doped into $ZnIn_2S_4$, more defect states would be introduced. Therefore, it is reasonable that the defect-related PL intensities were enhanced for the Cu^{2+}-doped samples compared with the undoped sample. As for the decrease of the PL intensity with the Cu^{2+} concentration above 0.5 wt%, it may be caused by the formation of CuS, though the XRD measurement did not detect the existence of the copper sulfide phase. In Eu-doped GaN,[40] a similar concentration quenching phenomenon was also observed, which was mainly attributed to the formation of EuN compound.

3.4. Band Structures. Figure 5A shows the band structure and the density of state (DOS) of $ZnIn_2S_4$. The density contour maps for the lowest unoccupied molecular orbitals (LUMO) and highest occupied molecular orbitals (HOMO) of $ZnIn_2S_4$ are shown in Figure 5B. We can observe clearly that both the top of valence band and the bottom of the conduct band lay at the G point of the Brillouin zone from Figure 5A. So the pure $ZnIn_2S_4$ crystal is a direct gap band semiconductor. The theoretical value of the direct gap at G is 0.4 eV, which is less than the experimental value of about 2.51 eV. Such an underestimation of the band gap is a well-known artifact of GGA. The density of states (Figure 5A) indicates that the S3p orbitals make a significant contribution to the valence band top of $ZnIn_2S_4$ and that the highest occupied molecular orbital (HOMO) levels are composed mainly of the hybridized S3p and Zn3d orbitals. The In5s orbitals locate at more negative energy levels than that of S3p orbitals and do not contribute much to the valence band top. The lowest unoccupied molecular orbital (LUMO) levels are composed mainly of the In5s5p and S3p orbitals. The Zn4s4p orbitals locate at more positive energy levels and do not contribute much to the conduction band bottom.

Based on the optical properties and DFT calculations, the schematic energy level diagram of Cu(X)-$ZnIn_2S_4$ is shown in Figure 6. As for $ZnIn_2S_4$, upon photoexcitation, electrons would transfer from the valence band (hybridized S3p and Zn3d orbitals) to the conduction band (hybridized In5s5p and S3p orbitals), leaving photogenerated holes in the valence band. As aforementioned, the PL emission has been known to be due to the photoluminescence transition from the sulfur-vacancy-related donor level or the conduction band to the valence band. Therefore, the energy difference between the absorption edge and the emission spectra of $ZnIn_2S_4$ can be explained. Taking the Cu doping into account, the t_2 state, splitting from discrete Cu3d levels, will form above the edge of valence band of $ZnIn_2S_4$, which is consistent with those reported by Peng[38] and Xu[41] in Cu-ZnS. A similar orbital-splitting phenomenon has been observed by Ye[42] and Zou[43] for Cr-3d and Ni-3d orbtials in $In_{12}NiCr_2Ti_{10}O_{42}$ and Ca_2NiWO_6. The t_2(Cu3d) level, produced by doping Cu^{2+} into $ZnIn_2S_4$, works as the donor level and acceptor level for photoexcitation and PL emission, respectively,[44] as shown in Figure 6. With the amount of Cu doped increasing, the t_2(Cu3d) level will be elevated farther from the

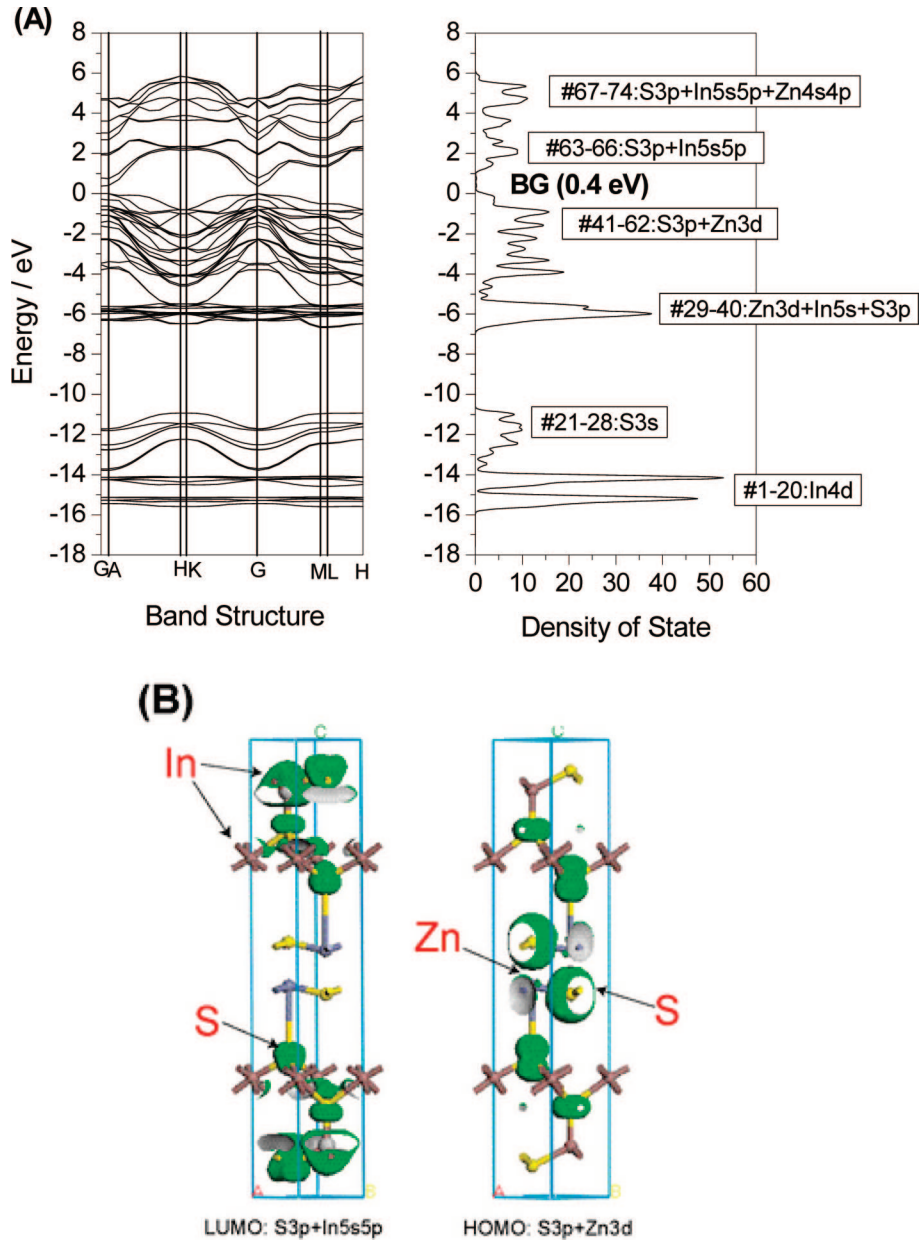

Figure 5. (A) Band structure and density of states for $ZnIn_2S_4$ calculated by the density functional method. (B) Density contour maps for the LUMO and HOMO of $ZnIn_2S_4$.

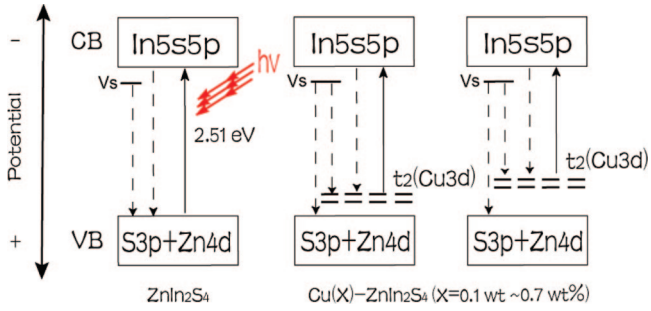

Figure 6. Schematic energy level diagram of Cu(X)-$ZnIn_2S_4$. Vs stands for sulfur vacancy.

valence band, which results in the redshift of absorption edge and PL emission for Cu(X)-$ZnIn_2S_4$.

3.5. Photocatalytic Activities of Cu(X)-$ZnIn_2S_4$. Figure 7 shows the dependence of photocatalytic H_2 evolution from an aqueous Na_2SO_3/Na_2S solution over Cu(X)-$ZnIn_2S_4$ under visible-light irradiation ($\lambda > 430$ nm). Either nondoped or Cu-

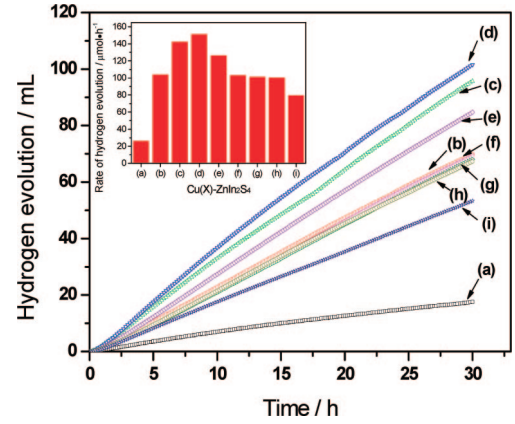

Figure 7. Photocatalytic H_2 evolution under visible-light irradiation over Cu(X)-$ZnIn_2S_4$; the values of X were (a) 0.0 wt%, (b) 0.1 wt%, (c) 0.3 wt%, (d) 0.5 wt%, (e) 0.7 wt%, (f) 0.9 wt%, (g) 1.2 wt%, (h) 1.6 wt%, (i) 2.0 wt%.

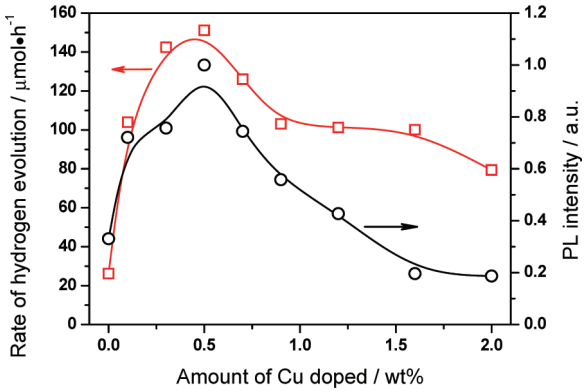

Figure 8. Dependence of photocatalytic activity for H_2 evolution and PL emission intensity over Cu(X)-$ZnIn_2S_4$, with X = 0.0 wt% to 2.0 wt%.

doped $ZnIn_2S_4$ was active and stable for splitting water to hydrogen. The rate of H_2 evolution over nondoped $ZnIn_2S_4$ was 26.1 μmol·h^{-1}. The apparent quantum yield at 420 nm was calculated to be 9.6% by eq 1. As the amount of doped Cu was increased, the photocatalytic activity of Cu(X)-$ZnIn_2S_4$ was increased, because the visible-light absorption band of Cu(X)-$ZnIn_2S_4$ grew.[11] The highest activity was obtained when 0.5 wt % of Cu was doped, the rate of hydrogen evolution reached at 151.5 μmol·h^{-1}, with the apparent quantum yield determined to be 14.2%. As the concentration of Cu doped was above 0.5 wt%, the activity was decreased, though the visible-light absorption band grew further. Such a similar dependence of photocatalytic H_2 evolution upon the amount of dopant has been observed for several other photocatalysts.[11,44,45] These observations indicated that the photocatalytic activites depended upon not only the visible-light absorption (i.e., band gap) but also some other factors. One of the reasons for the decrease in photocatalytic activity may be due to the impurity phase of CuS, resulted from the excess of Cu doping, as proved by XRD results. The CuS impurity may work as recombination sites between photogenerated electrons and holes. Another possible inactivation factor for the $ZnIn_2S_4$ doped with excessive Cu is that the layered structure could be destructed gradually with the amount of Cu increased further, as revealed by SEM images. Some perovskite photocatalysts with layered structure have also shown good photocatalytic activity for splitting water to hydrogen, as the dipole moment along layers seems to enhance the charge separation, resulting in high activity.[46,47]

Figure 8 shows the photocatalytic activity and photoluminescence intensity as a function of Cu content in the Cu(X)-$ZnIn_2S_4$. The change in photoluminescence intensity was concurrent to that in photocatalytic activity, as both photoluminescence intensity and photocatalytic activity reached the highest level when 0.5 wt % of Cu was doped. Photoluminescence depends on various factors such as the densities of photoexcited charges and recombination centers, the extent of nonradiation process, and the mobility of photoexcited charges.[44] It is difficult to determine which process is mainly responsible for changes in photoluminescence intensity with Cu content. However, in association with the change in photocatalytic activity, a plausible explanation can be made as follows. During the PL process, vacancies (such as sulfur vacancy) and defects can easily bind photoinduced electrons to form excitons, so that the PL signal can easily occur.[48] When Cu^{2+} ions were doped into $ZnIn_2S_4$, more vacancies (such as sulfur vacancy) or defect states would be introduced.[38] The larger the content of vacancy or defect, the stronger the PL signal. Meanwhile, an increase in Cu content not only raised the t_2 (Cu3d) level to narrow the band gap of Cu(X)-$ZnIn_2S_4$, which has been demonstrated by the UV−vis diffuse reflectance spectra, but also enhanced the density of the t_2 (Cu3d) levels and increased the concentration and the mobility of the photoexcited electrons.[44] These could be related to the enhancement of photocatalytic activity. However, further increase in the amount of Cu doped would result in the increased absorption to longer wavelength, which was likely due to the formation of CuS, as discussed previously. Thus, the CuS impurity weakened the photoluminescence,[40] as well as lowered photocatalytic activity of Cu-doped $ZnIn_2S_4$.[11]

4. Conclusions

In summary, we have synthesized a series of Cu-doped $ZnIn_2S_4$ photocatalysts by a simple hydrothermal method. The photocatalytic activity of $ZnIn_2S_4$ was remarkably enhanced by Cu doping. The optimized Cu (0.5 wt%)-doped $ZnIn_2S_4$ photocatalyst showed the highest activity for splitting water into H_2, with the rate of hydrogen evolution to be 151.5 μmol·h^{-1}. With increasing concentration of Cu doped, the UV−vis spectra and PL emission peak were systematically shifted to longer wavelength. Moreover, there were certain intrinsic relationships between the PL emission intensity and photocatalytic activity of Cu-doped $ZnIn_2S_4$. That is to say, the change in photoluminescence intensity was concurrent to that in photocatalytic activity, both depending on the increasing concentration of Cu doped.

Acknowledgment. The authors gratefully acknowledge the financial support of the National Natural Science Foundation of China (No.50521604) and National Basic Research Program of China (No.2003CB214500). The authors also would like to thank the molecular simulating platform and National High Performance Computing Center (Xi'an) at Xi'an Jiaotong University for the calculation resource support.

References and Notes

(1) Domen, K.; Kudo, A.; Ohnishi, T. *J. Catal.* **1986**, *102*, 92.
(2) Hwang, D. W.; Kim, H. G.; Kim, J.; Cha, K. Y.; Kim, Y. G.; Lee, J. S. *J. Catal.* **2000**, *193*, 40.
(3) Kato, H.; Asakura, K.; Kudo, A. *J. Am. Chem. Soc.* **2003**, *125*, 3082.
(4) Sato, J.; Saito, N.; Yamada, Y.; Maeda, K.; Takata, T.; Kondo, J. N.; Hara, M.; Kobayashi, H.; Domen, K. *J. Am. Chem. Soc.* **2005**, *127*, 4150.
(5) Kim, H. G.; Hwang, D. W.; Lee, J. S. *J. Am. Chem. Soc.* **2004**, *126*, 8912.
(6) Maeda, K.; Teramura, K.; Lu, D.; Takata, T.; Saito, N.; Inoue, Y.; Domen, K. *Nature* **2006**, *440*, 295.
(7) Ritterskamp, P.; Kuklya, A.; Wüstkamp, M.; Kerpen, K.; Weidenthaler, C.; Demuth, M. *Angew. Chem., Int. Ed.* **2007**, *46*, 7770.
(8) Niishiro, R.; Kato, H.; Kudo, A. *Phys. Chem. Chem. Phys.* **2005**, *7*, 2241.
(9) Kudo, A.; Sekizawa, M. *Catal. Lett.* **1999**, *58*, 241.
(10) Kudo, A.; Sekizawa, M. *Chem. Commun.* **2000**, *15*, 1371.
(11) Tsuji, I.; Kudo, A. *J. Photochem. Photobiol. A* **2003**, *156*, 249.
(12) Zou, Z. G.; Ye, J. H.; Sayama, K.; Arakawa, H. *Nature* **2001**, *414*, 625.
(13) Bubler, N.; Meier, K.; Reber, J. F. *J. Phys. Chem.* **1984**, *88*, 3261.
(14) Naman, S. A.; Grätzel, M. *J. Photochem. Photobiol. A* **1994**, *77*, 249.
(15) Inoue, T.; Watanabe, T.; Fujishima, A.; Honda, K. *J. Electrochem. Soc.* **1977**, *124*, 719.
(16) Shangguan, W.; Yoshida, A. *J. Phys. Chem. B* **2002**, *106*, 12227.
(17) Shen, S.; Guo, L. *J. Solid State Chem.* **2006**, *179*, 2629.
(18) Shen, S.; Guo, L. *Mater. Res. Bull.* **2008**, *43*, 437.
(19) Tsuji, I.; Kato, H.; Kobayashi, H.; Kudo, A. *J. Am. Chem. Soc.* **2004**, *126*, 13406.
(20) Tsuji, I.; Kato, H.; Kudo, A. *Angew. Chem., Int. Ed.* **2005**, *44*, 3565.
(21) Jang, J. S.; Choi, S. H.; Shin, N.; Yub, C.; Lee, J. S. *J. Solid State Chem.* **2007**, *180*, 1110.

(22) Liu, G.; Zhao, L.; Ma, L.; Guo, L. *Catal. Commun.* **2008**, *9*, 126.
(23) Romeo, N.; Dallaturca, A.; Braglia, R.; Sberveglieri, G. *Appl. Phys. Lett.* **1973**, *22*, 21.
(24) Seo, W. S.; Otsuka, R.; Okuno, H.; Ohta, M.; Koumoto, K. *J. Mater. Res.* **1999**, *14*, 4176.
(25) Romeo, N.; Tarricone, L.; Zanotti, L. *Il Nuovo Cim. D* **1983**, *2*, 2007.
(26) Lei, Z.; You, W.; Liu, M.; Zhou, G.; Takata, T.; Hara, M.; Domen, K.; Li, C. *Chem. Commun.* **2003**, *17*, 2142.
(27) Gou, X.; Cheng, F.; Shi, Y.; Zhang, L.; Peng, S.; Chen, J.; Shen, P. *J. Am. Chem. Soc.* **2006**, *128*, 7222.
(28) Shen S.; Zhao L.; Guo L. *Mater. Res. Bull.*, 2008, doi:10.1016/j.materresbull.2008.03.027.
(29) Shen S.; Zhao L.; Guo L. *Int. J. Hydrogen Energy*, 2008, doi:10.1016/j.ijhydene.2008.05.043.
(30) Segall, M. D.; Lindan, P. J. D.; Probert, M. J.; Pickard, C. J.; Hasnip, P. J.; Clark, S. J.; Payne, M. C. *J. Phys.: Condens. Matter* **2002**, *14*, 2717.
(31) Vanderbilt, D. *Phys. Rev. B* **1990**, *41*, 7892.
(32) Lei, Z.; Ma, G.; Liu, M.; You, W.; Yan, H.; Wu, G.; Takata, T.; Hara, M.; Domen, K.; Li, C. *J. Catal.* **2006**, *237*, 322.
(33) Shionoya, S.; Tamoto, Y. *J. Phys. Soc. Jpn.* **1964**, *19*, 1142.
(34) Konta, R.; Ishii, T.; Kato, H.; Kudo, A. *J. Phys. Chem. B* **2004**, *108*, 8992.
(35) Miyauchi, M.; Takashio, M.; Tobimatsu, H. *Langmuir* **2004**, *20*, 232.
(36) Spanhel, I.; Anderson, M. A. *J. Am. Chem. Soc.* **1991**, *113*, 2826.
(37) Castro, S. L.; Bailey, S. G.; Raffaelle, R. P.; Banger, K. K.; Hepp, A. F. *J. Phys. Chem. B* **2004**, *108*, 12429.
(38) Peng, W. Q.; Cong, G. W.; Qu, S. C.; Wang, Z. G. *Opt. Mater.* **2006**, *29*, 313.
(39) Ghosh, P. K.; Ahmed, Sk. F.; Jana, S.; Chattopadhyay, K. K. *Opt. Mater.* **2007**, *29*, 1584.
(40) Bang, H.; Morishima, S.; Sawahata, J.; Seo, J.; Takiguchi, M.; Tsunemi, M.; Akimoto, K.; Nomura, M. *Appl. Phys. Lett.* **2004**, *85*, 227.
(41) Xu, S. J.; Chua, S. J.; Liu, B.; Gan, L. M.; Chew, C. H.; Xu, G. Q. *Appl. Phys. Lett.* **1998**, *73*, 478.
(42) Wang, D.; Zou, Z.; Ye, J. *Chem. Phys. Lett.* **2005**, *411*, 285.
(43) Li, D.; Zheng, J.; Zou, Z. *J. Phys. Chem. Solids* **2006**, *67*, 801.
(44) Arai, N.; Saito, N.; Nishiyama, H.; Domen, K.; Kobayashi, H.; Sato, K.; Inoue, Y. *Catal. Today* **2007**, *129*, 407.
(45) Nishimoto, S.; Matsuda, M.; Miyake, M. *Chem. Lett.* **2006**, *35*, 308.
(46) Kudo, A.; Kato, H.; Nakagawa, S. *J. Phys. Chem. B* **2000**, *104*, 571.
(47) Hwang, D. W.; Kim, H. G.; Lee, J. S.; Kim, J.; Li, W.; Oh, S. H. *J. Phys. Chem. B* **2005**, *109*, 2093.
(48) Jing, L.; Qu, Y.; Wang, B.; Li, S.; Jiang, B.; Yang, L.; Fu, W.; Fu, H.; Sun, J. *Sol. Energy Mater. Sol. Cells* **2006**, *90*, 1773.

JP804525Q